INTERNATIONAL JOURNAL FOR NUMERICAL METHODS IN FLUIDS, VOL. 20, 713–741 (1995)

FINITE ELEMENT/FINITE VOLUME SOLUTIONS OF FULL POTENTIAL, EULER AND NAVIER–STOKES EQUATIONS FOR COMPRESSIBLE AND INCOMPRESSIBLE FLOWS

M. HAFEZ

Department of Mechanical and Aeronautical Engineering, University of California, Davis, Davis, CA 95616, U.S.A.

SUMMARY

A cell-vertex finite volume formulation, using local finite element approximations to calculate fluxes through an auxiliary mesh (control volumes) is used to solve inviscid and viscous compressible flow equations on unstructured grids. Non-linear artificial viscosity methods are adopted to avoid decoupling and capture shock waves. Artificial time-dependent terms are augmented if needed, to guarantee convergence of common iterative procedures to a steady-state solution. The incompressible limit of compressible flow equations is studied. A unified approach for solving both compressible and incompressible flow problems is proposed. Also some results of a zonal formulation with different governing equations in different regions are presented. Applications to the solution of Maxwell's equations for wave propagation and scattering are discussed in an appendix.

KEY WORDS: inviscid and viscous flows; unstructured grids

1. INTRODUCTION

In this paper, simple methods to calculate compressible flows are presented. The basic idea is to modify the governing differential equations with artificial viscosity and artificial time-dependent terms and then apply standard discretization procedures suitable for unstructured grids to obtain a system of non-linear algebraic equations which can be solved iteratively in an efficient manner.

Both finite volumes and finite elements methods can be used to obtain discrete analogues of the governing equations. Conservative discretization can be achieved with either cell-centered or cell-vertex finite volumes. The latter, however, is similar in many aspects to finite element methods.[1,2]

In the present work, the augmented equations are written in conservation form and are integrated over control volumes (constructed around each node and cover all the domain as shown in Figure 1) via Gauss and Stokes theorems. The line (and surface) integrals are numerically evaluated based on local finite element approximations using the nodal values of the unknowns. If linear shape functions are used, the scheme is closely related to the Galerekin finite element method. Applications to full potential, Euler, Navier–Stokes, as well as Maxwell's equations are considered. Accurate treatments of boundary conditions are examined.

In the following, the formulation of the problem and the corresponding numerical methods are discussed. Finally, some preliminary results are presented together with some concluding remarks.

CCC 0271–2091/95/080713–29

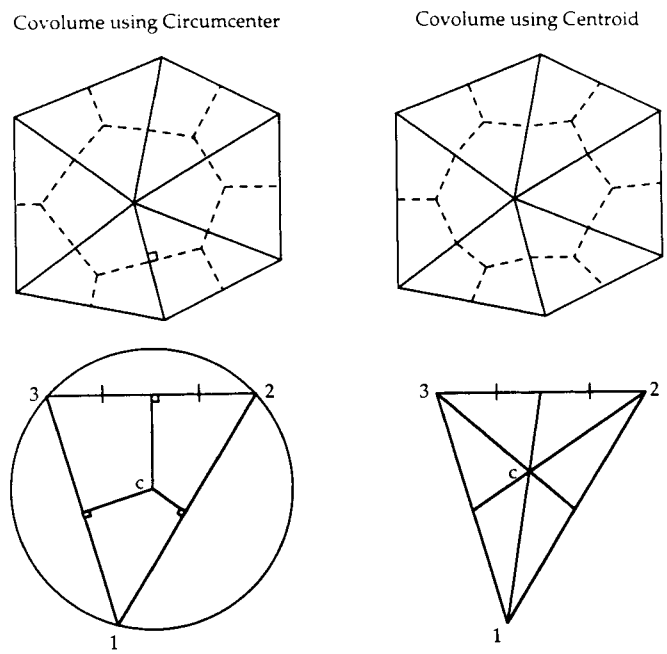

Figure 1. Constructions of control volumes in two dimensions

2. SOLUTIONS OF POTENTIAL EQUATION

The inviscid limit of Navier–Stokes equations, as Reynolds number approaches infinity, is the Euler equations reflecting conservation of mass, momentum and energy and allowing in general for variation of entropy and vorticity in the flow field. For external aerodynamic problems of a smooth body at near design conditions in a uniform flow, the vorticity almost vanishes outside a thin viscous layer around the body and in the wake. Hence, such an irrotational flow can be described by a potential. Furthermore, the flow can be assumed isentropic leading to an explicit relation between the density and the pressure. Under these conditions, the Euler equations can be replaced by a simpler model of one equation in one variable. The momentum equations are not satisfied in general, with the assumptions of zero vorticity and constant entropy. Indeed, the model is not physically valid when these assumptions are grossly violated. Nevertheless, it is useful even for transonic flows with shock waves.

The full potential equation is simply the conservation of mass with the velocity represented as the gradient of a potential. The isentropic relation combined with the energy equation (or Bernoulli's law) provides an expression for the density in terms of the speed. More precisely, the governing equation for the potential ϕ is

$$\nabla \cdot \bar{\rho} \nabla \phi = 0 \tag{1}$$

where

$$\bar{\rho} = \left(1 - \frac{\gamma - 1}{2} M_\infty^2 (1 \nabla \phi 1^2 - 1)\right)^{1/(\gamma - 1)} \tag{2}$$

In the above expression, M_∞ is the free stream Mach number and $\gamma = 1{\cdot}4$ for air. Also, the density and the velocity are normalized by their free stream values.

At a solid surface, the normal velocity component ϕ_n must vanish (the tangency condition). For a lifting aerofoil, the Kutta–Joukowski condition must be imposed which guarantees that the flow leaves the aerofoil in a direction bisecting the trailing edge angle. In the far field, an irrotational vortex must be added to the uniform flow. The strength of the vortex, Γ, is the jump of the potential at the trailing edge and it is constant along a cut extending to the outer boundary of the domain of the calculations.

The non-linear potential equation admits a discontinuous solution with (isentropic) jump conditions. To exclude expansion shocks, weak solutions must satisfy a generalized entropy inequality.

It turns out that even with the Kutta–Joukowski condition and entropy inequality satisfied, the solution is not necessarily unique. Multiple solutions can be numerically calculated for some lifting aerofoils with shocks, where the lift coefficient is no longer a single-valued function of the angle of attack. After this non-uniqueness problem was discovered, basic research on potential flows has almost stopped except at Boeing Company where potential flow codes are still in use till today.[3]

So, the question is: How can the potential flow model be used for practical problems in industry, if it suffers from such a major deficiency? To answer this question, one must consider the potential flow model as an approximation of high Reynolds number flow outside the shear layers. For example, potential flow solvers must be coupled with boundary layer calculations to satisfy the no slip boundary condition at a solid surface. So, even the potential flow model, by itself, breaks down, the viscous/inviscid interaction procedure including the wake and its curvature effects may provide a reasonable answer.

In general, the non-uniqueness of the solution of the steady equations may be an indication that the physical solution is time dependent and one must examine the asymptotic solution of the unsteady equations.

Finally, the probability of having non-unique solutions for three-dimensional flows around practical wings is almost zero, as proved by the production codes at Boeing for the last two decades.

The formulation of the three-dimensional problem is more complicated since the wake should not be fixed, otherwise it will carry a load. Usually, for convenience, the wake is assumed to be planar. At each cross-section, the circulation is calculated and kept a constant along the wake from the trailing edge to the outer boundary, as in the small disturbance theory. (A more exact treatment of the wake as a contact discontinuity which can be fitted to guarantee the pressure is continuous, has been attempted by some researchers to study the roll-up process with a model for the core of the vortex.)

Numerical methods and results

The main features of the present work, see References 4, 5 for more details, can be summarized as

1. A frontal surface and tetrahedral grid generation algorithm[6] is used to generate fully unstructured grids. The grid is also easily adapted based on the gradient of the solution.
2. A combination of second and first-order upwind flux scheme,[7,8] is limited similar to Jameson's 'USLIP' construction.[9]

3. A conjugate gradient squared algorithm (CGSTAB)[10] is chosen for the solution of the linear system of equations at each Newton's iteration, with a symmetric successive over relaxation (SSOR) procedure as a preconditioner.

The following remarks can be made:

a. Since linear elements are used, with the potential stored at the nodes, the Cartesian velocity components, and hence the density, are constant in each element. For pure subsonic flows, where the equation is elliptic, no artificial viscosity is needed and the same compact scheme results from finite volumes, or Galerekin finite elements methods. With a proper linearization of the density, the convergence of the Newton's iteration is quadratic. Even with lagging the density, the convergence rate is acceptable.
b. For transonic flows, the density is biased or retarded only in the supersonic region, introducing artificial dissipation, necessary for the numerical stability of the calculations. The values of the flux in the nearby upwind elements are used. Thus, linearization of the biased or retarded density leads to a non-symmetric Jacobian. We notice that the governing equation is of mixed type and to help the convergence time-dependent terms (ϕ_{tt}) and (ϕ_{st}) similar to those terms of the unsteady transonic flow equation are introduced. Upwind discretization of the streamwise derivative $\partial/\partial s$ desymmetrizes the Jacobian matrix and is switched off in the subsonic flow region.
c. For two-dimensional flows, the first-order version of the present scheme is similar to that of Pelz and Jameson[2] including the artificial viscosity produced via the streamwise upwinding.

Numerical results (obtained by D. Kinney) for M6 wing at $M_\infty = 0{\cdot}839$ and $\alpha = 3{\cdot}06°$ are plotted in Figure 2. Figure 2(a) shows coarse and refined grids. The grids vary from 100 000 to 350 000 nodes. The density contours are shown in Figure 2(b) and the surface pressure distribution at 90 per cent of the semi-span are plotted in Figure 2(c). (The experimental data are included only as a reference, no boundary layer or wall interference effects are accounted for).

The incompressible limit of the compressible potential flow equations. One can consider a flow of air, at low Mach numbers as incompressible. The Mach number is defined as

$$M = q/a \tag{3}$$

where

$$a^2 = \left.\frac{\partial p}{\partial \rho}\right|_{\Delta s = 0} \tag{4}$$

hence as $\delta\rho$ vanishes, the speed of sound (a) approaches infinity and the Mach number vanishes. Roughly speaking, the ratio of the relative change of the density to the relative change of the velocity is of the order of the Mach number squared $\delta\rho/\rho/\delta q/q = O(M^2)$.

It is clear as the free stream Mach number goes to zero, the full potential equation reduces to a Laplacian since the density approaches a constant. On the other hand, the Bernoulli's law of compressible flow reads:

$$\frac{\gamma}{\gamma - 1}\frac{p}{\rho} + \frac{1}{2}q^2 = \frac{\gamma}{\gamma - 1}\frac{p_\infty}{\rho_\infty} + \frac{1}{2}q_\infty^2 = H_\infty \tag{5}$$

Hence, to obtain the incompressible limit the factor $\gamma/(\gamma - 1)$ must approach 1 or γ approaches infinity.

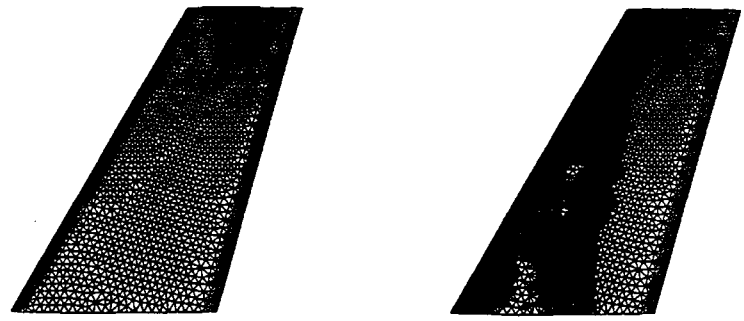

Grid 0 Grid 1

Grid 2 Grid 3

(a)

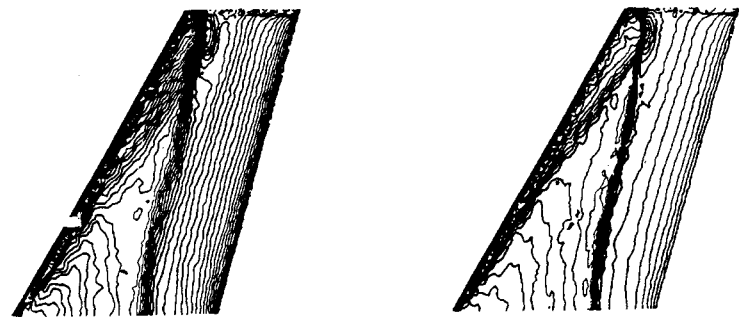

Grid 0 Grid 1

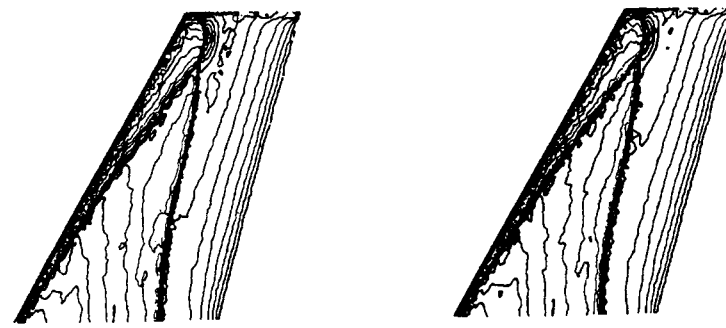

Grid 2 Grid 3

(b)

Figure 2. (a, b)

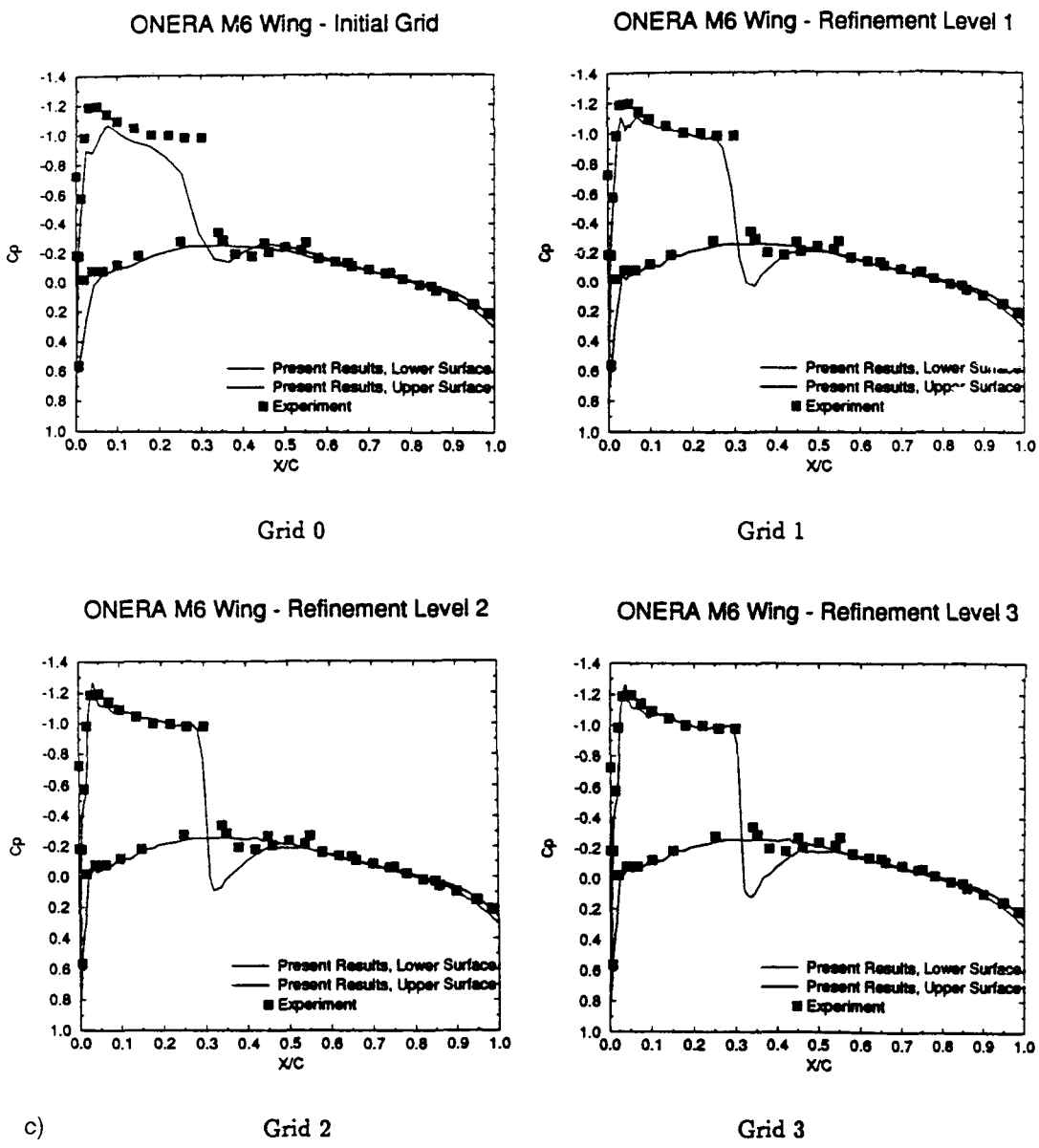

Figure 2. (a) Grids, (b) density contours and (c). C_p at 90 per cent semi-span, for M6 wing, Mach 0·839, 3·06°

We can avoid this difficulty if we deal instead with the pressure coefficient, C_p defined as

$$C_p = \frac{p - p_\infty}{(1/2)\rho_\infty q_\infty^2} = 2(\bar{p} - \bar{p}_\infty) \tag{6}$$

where $\bar{p}$ is a normalized pressure. The isentropic relation in terms of $\bar{p}$ and $\bar{\rho}$ is given by

$$\bar{p} = \bar{\rho}^\gamma / \gamma M_\infty^2 \tag{7}$$

Hence,

$$C_{p_{\text{comp}}} = 2\left(\frac{\bar{\rho}^{\gamma}}{\gamma M_{\infty}^2} - \frac{1}{\gamma M_{\infty}^2}\right) \tag{8}$$

substituting for $\bar{\rho}$, one obtains

$$C_{p_{\text{comp}}} = 2\left(\frac{\left[1 - \dfrac{\gamma - 1}{2} M_{\infty}^2 (\bar{q} - 1)\right]^{\gamma/\gamma - 1} - 1}{\gamma M_{\infty}^2}\right) \tag{9}$$

Using a binomial expansion for small Mach numbers, the above expression reduces to

$$C_{p_{\text{comp}}} = (1 - q^2) + M_{\infty}^2 \delta \tag{10}$$

where $(M_{\infty}^2 \delta)$ represents the rest of the terms in the expansion. Therefore,

$$\lim_{M_{\infty}^2 \to 0} (C_{p_{\text{comp}}}) = C_{p_{\text{incomp}}} \tag{11}$$

The above analysis holds for unsteady flows (with uniform upstream conditions) as well, if $\bar{q}^2$ is replaced by

$$\bar{q}^2 + 2\phi_t$$

The conclusion is: potential codes for compressible flows can be used for the simulation of incompressible flows (with zero Mach number) with a modified form of the pressure coefficient, based on a binomial expansion. The situation is more complicated for Euler and Navier–Stokes equations as will be discussed later.

3. SOLUTIONS OF EULER EQUATIONS

Recently, there have been intensive efforts dedicated to develop efficient solvers, based on the conservation laws, to simulate flows over complex geometrics. For strong shocks, the entropy jump cannot be neglected. Furthermore, if the shock is curved the entropy jump varies along the shock generating a vorticity field and the potential flow model cannot be used by itself. There are also many applications where the flow field is inherently rotational as for example if a strong gust exists, or, for the case of a tail in the wake of a wing. Euler codes are also needed to capture contact discontinuities, a more difficult task than capturing shock waves. Moreover, Euler calculations can shed some light on the properties of shear flows in the limit of high Reynolds numbers. At any rate, an efficient and accurate Euler Code is a necessary step toward developing practical Navier–Stokes codes.

The conservation of mass, momentum and energy for unsteady flows is a natural formulation based on a hyperbolic system of equations to obtain asymptotically, for large time, a steady-state solution (if it exists). It is conceivable, however, that one can construct a more efficient iterative algorithm (as in the pseudo-time dependent approach[11]) to solve the steady equations. In some cases, for example, if an implicit procedure is used, the obtained solution may not be stable, or in other words, it is physically unrealizable. Moreover, since the steady equations are non-linear, they may admit multiple solutions. Recently, Jameson[12] has calculated non-unique solutions of Euler equations for certain aerofoils. Hence, the conclusion of a previous study by Salas *et al.*,[13] that the non-uniqueness problem of the full potential equation is due to the assumptions that the flow is irrotational and isentropic and the exact inviscid (Euler) model does not have this

anomaly, is no longer valid. The non-uniqueness problem of the steady equations may be an indication that the steady-state limit of the time-dependent equations does not exist.

Other types of non-uniqueness may result if the formulation is not well-posed. Recently, Pulliam[14] calculated a lifting solution over a cylinder and an ellipse in low subsonic flows at a small angle of attack using several Euler codes. For this problem, analytical solutions of the potential equation are available. They are also exact solutions of Euler equations. On the discrete level, however, Euler calculations are contaminated with the artificial dissipation necessarily for numerical stability. Hence, depending on the level of artificial vorticity generated due to the artificial dissipation and the numerical treatment of boundary conditions, circulation and lift can be developed in the discrete solution. In Reference 15, Hafez and Brucker constructed a scheme for incompressible Euler equations which conserved vorticity. It was shown therefore that a discrete potential existed and numerical results for the cylinder, and the ellipse problems with zero lift and drag (up to machine accuracy) were presented.

It was also realized that other solutions with lift (and zero drag) existed. In Reference 16, Winterstein and Hafez argued that the formulation is not well-posed. Obviously, an irrotational vortex (of any finite strength) can be added to the solution satisfying the tangency condition at the solid surface with a uniform flow at infinity, since the velocity component due to the vortex dies like $1/r$, where r is the distance from the centre of the cylinder. By specifying the rear stagnation point on the surface of the body, one can obtain a solution with a certain lift. In particular, a zero lift solution, can be easily calculated, as demonstrated in References 16 and 17. Simply, as in potential flows, a Kutta–Joukowski condition is needed for Euler calculations over smooth bodies. For aerofoils with sharp trailing edges, the artificial viscosity (necessary for numerical stability) forces the flow to leave the trailing edge smoothly. There is no guarantee, however, that the flow leaves tangent to the side of lower entropy, as the inviscid model requires. Therefore, the treatment of the sharp trailing edge in existing Euler codes may not be completely satisfactory. In the following, some Euler calculations over aerofoils and smooth bodies, based on finite element/finite volume discretization using unstructured grids will be examined.

Numerical methods and results

The Euler equations, in two dimensions, written in conservation form, and using standard notations, read

$$F_x + G_y = 0 \tag{12}$$

where F and G are the fluxes in the x and y directions. Using Gauss theorem, the above equations are integrated over the control volumes, constructed around the nodes, to yield a system of equations reflecting the balance of fluxes. In each element, the line integral of the fluxes is numerically evaluated using a local approximation based on the representation of the variables in terms of their nodal values. For example, in triangles, the variables vary linearly and a trapezoidal rule can be employed to calculate each segment of the line integral and all the relevant contributions are assembled, for each node, to obtain the system of discrete equations. To avoid decoupling and to capture solution discontinuities, artificial viscosity terms are added to Euler equations and are properly discretized. The simplest form of artificial viscosity is the Laplacian, with a coefficient proportional to the grid size. The result, however, is at best first-order accurate. A higher-order viscosity (fourth-order derivatives) can be used for smooth flows, but it does not guarantee non-oscillatory solutions for flows with shocks. A blending of Laplacian and biharmonic operators is used by Jameson *et al.* very successfully.[18] To avoid the wiggles in the shock region, the fourth-order derivative terms are switched off while the second-order derivative terms

are only active in this large gradient region. The scheme has been reformulated in terms of flux limiters and its applications on unstructured grids has been demonstrated for two- and three-dimensional flows.[8]

One problem of this scheme is the numerical boundary conditions required for the solution of the higher-order system. In the early applications, extrapolations from interior nodes were used to obtain values at ghost points. This process led to inaccurate results as discussed in Reference 13. A careful treatment of boundary conditions is necessary to avoid generation of artificial vorticity as discussed in References 15 and 16.

Other alternatives are Lax–Wendroff and least-squares schemes. MacCormack's version of Lax–Wendroff scheme[19] has been used extensively for more than two decades. A new implicit version, due to Lerat,[20] gives excellent results on regular grids. A finite element analogue of a Lax–Wendroff scheme was proposed by Donea.[21] Least-squares methods have been studied by Hughes[22] and Jiangand Povinelli.[23] The Taylor–Galerkin and the least-squares Galerkin methods are compared in Reference 24 for transonic flow calculations. It is shown that the two methods can be identical if the equations are written as a symmetric system of hyperbolic equations (i.e., if the entropy variables are used).

In the present study, a simplified partial least-squares method is employed. Following Winterstein and Hafez,[16] the continuity equation is augmented by the Lapalacian of the pressure balanced by some extra terms. The total expression is obtained via minimizing the integral of the sum of the squares of the momentum equations (assuming mass is conserved) with respect to the pressure. For smooth flows, this expression vanishes on the differential level, but its discrete analogue is not necessarily zero. Also, the momentum equations are augmented by extra terms providing upon discretization higher order, streamwise, artificial diffusion. For example, the minimization of the integral of the square of the x-momentum equation with respect to u, the velocity component in the x direction, assuming mass is conserved and the pressure and the density are known, yields an expression containing second derivatives of u, balanced by pressure terms. Again, this total expression vanishes for smooth flows on the differential level. The y-momentum equation is treated similarly. The total enthalpy is assumed constant, otherwise the energy equation with its corresponding augmented terms is used.

The present formulation is simpler than those of the Lax–Wendroff or full least-squares methods since the momentum balance in each direction is dealt with separately as a scalar equation. Using the present finite element/finite volume discretization procedure, no cross-wind diffusion, in the momentum equations, is produced. Moreover, since only second order derivatives appear in these extra augmented terms, the discrete scheme is still compact relating the unknowns at a node to the unknowns at the nearest surrounding nodes. Also, since the extra-augmented terms are related to the original equations, the extra numerical boundary conditions are obtained simply by enforcing the original first-order equations at the boundaries. More precisely, the area integrals of the artificial viscosity terms in the continuity equation are reduced via Gauss's theorem to line integrals of first-order equations along the sides of the control volume. These line integrals are ignored at solid surfaces. The extra terms added to the momentum equations are derivatives along the flow direction, and since the body is a streamline, no extra boundary conditions are needed for the evaluation of these terms. Therefore, only physical boundary conditions are required in the present method.

For blunt bodies, however, another approach is recommended. The pressure at a boundary node is obtained using the normal momentum equation written in terms of R, the radius of curvature of the solid surface. Similarly, the vorticity (ω) can be written in terms of R and if the vorticity is zero at the solid surface, as in subsonic flows with uniform upstream conditions, the speed at a boundary node can be easily determined.

In general, ω does not vanish at the solid surface. It can be calculated, however, based on Crocco's relation. (For constant total enthalpy case, ω is related to the normal derivative of the entropy.) Once the surface pressure and speed are known, the density is evaluated from the total enthalpy. Imposing the vorticity at the solid surface, leads to a more accurate solution. No artificial viscosity is needed at the boundary, and hence the solution is not contaminated with artificial vorticity generated because of the numerical boundary conditions required for the higher-order derivatives. Numerical experiments confirm this conclusion as will be shown later.

The discrete equations for all internal and boundary nodes are then linearized using Newton's method. The diagonal terms of the Jacobian are augmented with $A/\Delta t$, where A is the area of the control volume and Δt is an artificial time step to help the convergence of the iterative procedure which is employed to calculate the correction. Once the solution is updated, the residual and the Jacobian are evaluated and the process is repeated until convergence. For semi-unstructured grids where rings of nodes can be identified although the number of nodes varies from one ring to another, a zebra or a block relaxation algorithm is used where a periodic black tridiagonal solver is required. The convergence of the iterative process can be accelerated using for example GMRES techniques.

The results for compressible flows over an ellipse (6:1) are presented. The rear stagnation point is fixed as discussed in Reference 16. The case of $M_\infty = 0{\cdot}2$ and $\alpha = 5°$, calculated by Pulliam,[14] is studied. A grid of 128 nodes on the surface and 50 rings is used with a uniform flow as an initial guess. The pressure contours, the surface pressure distribution and the convergence history are plotted in Figures 3(a), 3(b) and 3(c), respectively. The lift and drag coefficients are of order 10^{-4} and the maximum change in entropy is $\sim 2 \times 10^{-3}$. The results of the calculations of subsonic flows $M_\infty = 0{\cdot}2$ over a lifting NACA 0012 aerofoil at 10 and 20° are shown in Figures 3(d) and 3(e). The body is discretized with 152 nodes and the outer boundary is placed 20 chords away. At the trailing edge, the blunt body conditions are substituted with the no flux-boundary conditions. No flow separation is detected. The lift coefficients are 1·2 and 2·39, respectively, and the drag coefficient is of the order of the truncation error.

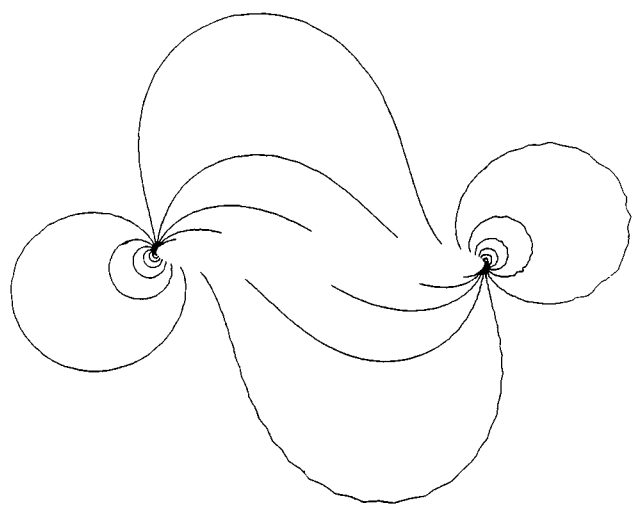

(a)

Figure 3. (a)

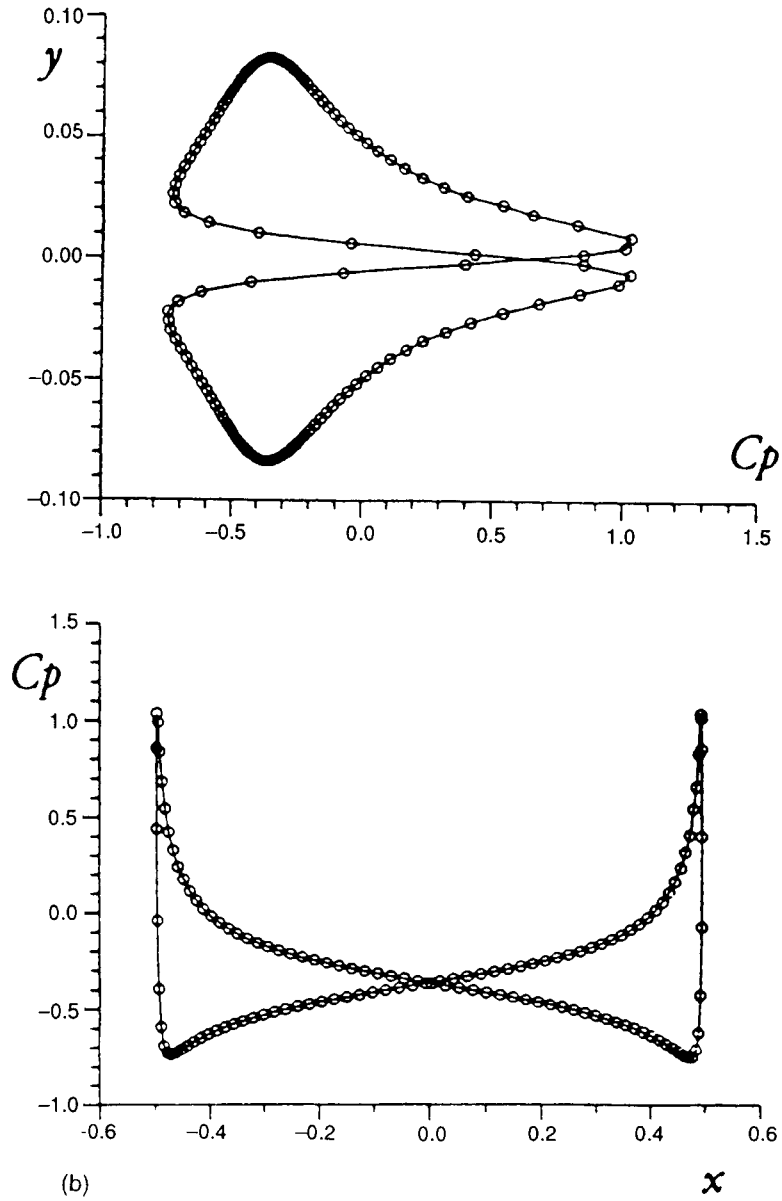

Figure 3. (b)

To obtain non-oscillatory solutions, for transonic flows, more artificial viscosity, in terms of a Laplacian of the pressure, is added to the continuity equation, without the associated balancing terms, in the shock region. Several combinations of balanced and unbalanced Laplacian are addressed in a joint effort of Habashi using a standard Galerkin method with bilinear elements in Reference 25.

In Figure 3(f), the surface pressure distribution for the case of $M_\infty = 0{\cdot}8$ and zero angle of attack is plotted. The convergence history is shown in Figure 3(g). The results for two lifting cases

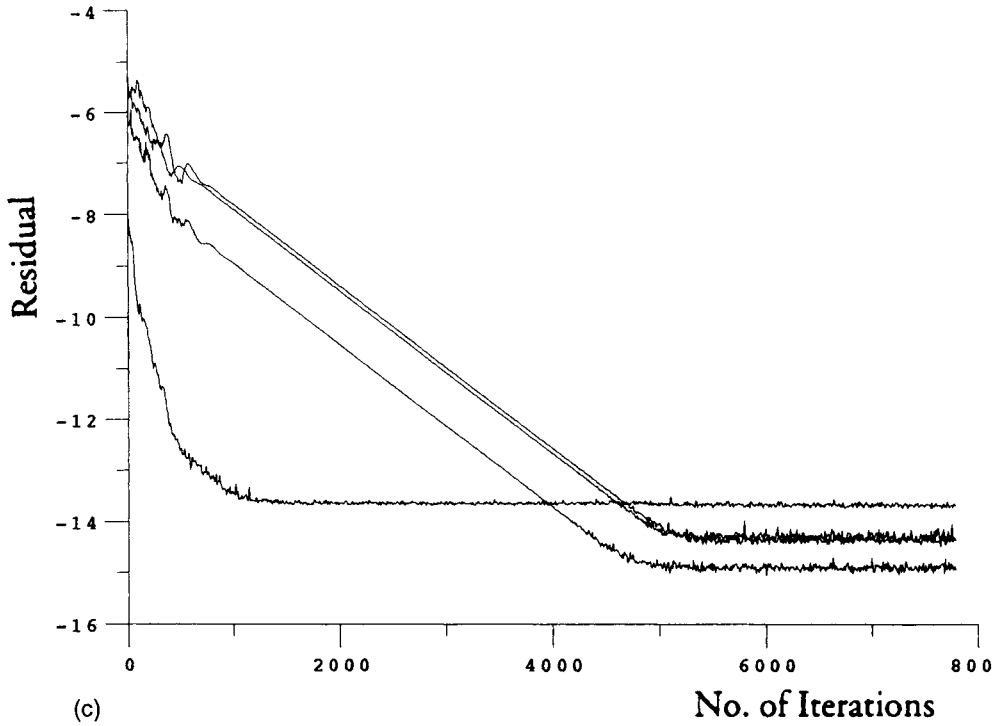
Residual
-4
-6
-8
-10
-12
-14
-16
0
2000
4000
6000
8000
No. of Iterations
(c)

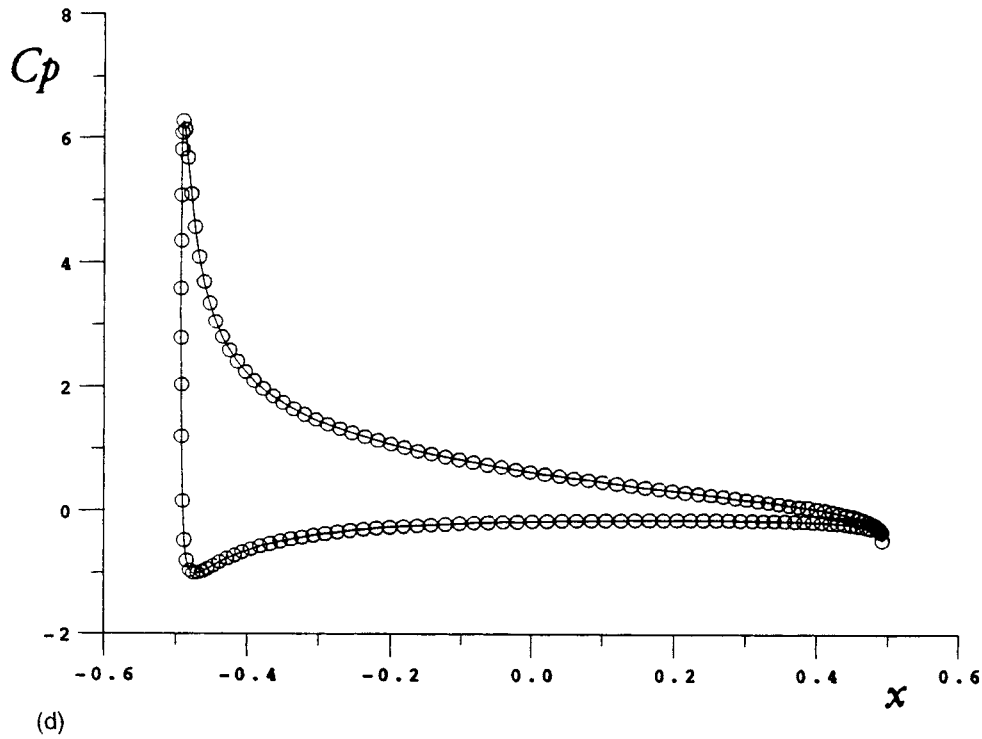
Cp
8
6
4
2
0
-2
-0.6
-0.4
-0.2
0.0
0.2
0.4
0.6
x
(d)

Figure 3. (c, d)

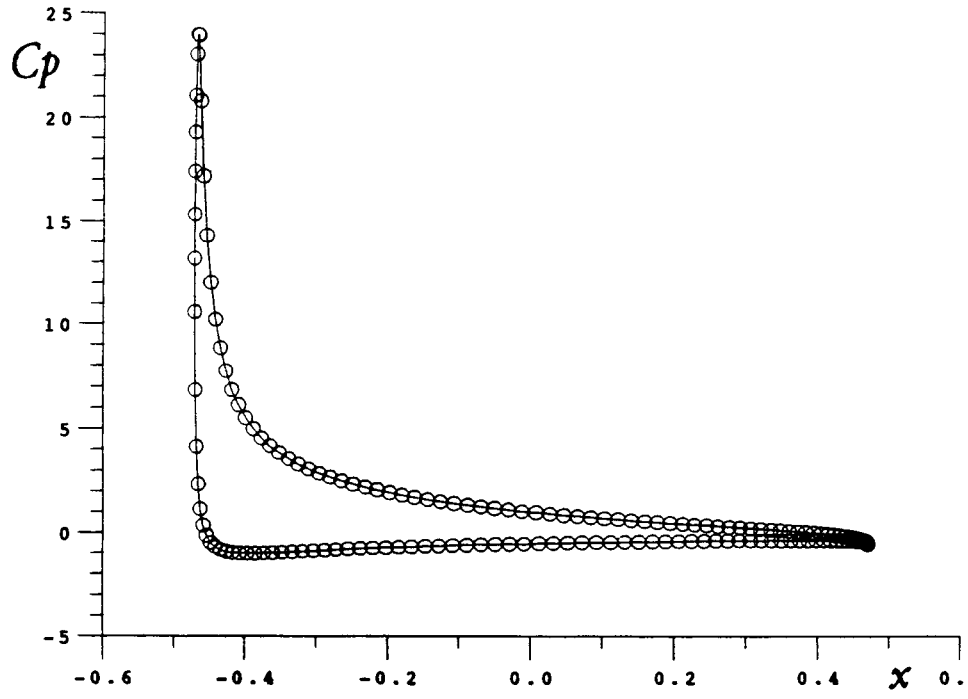

(e)

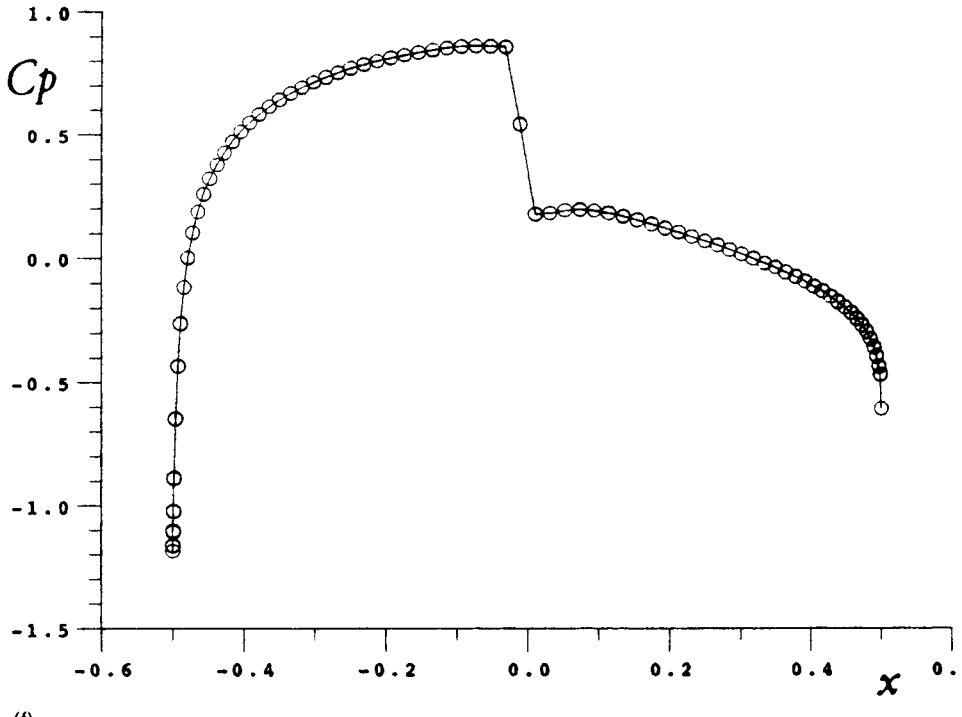

(f)

Figure 3. (e, f)

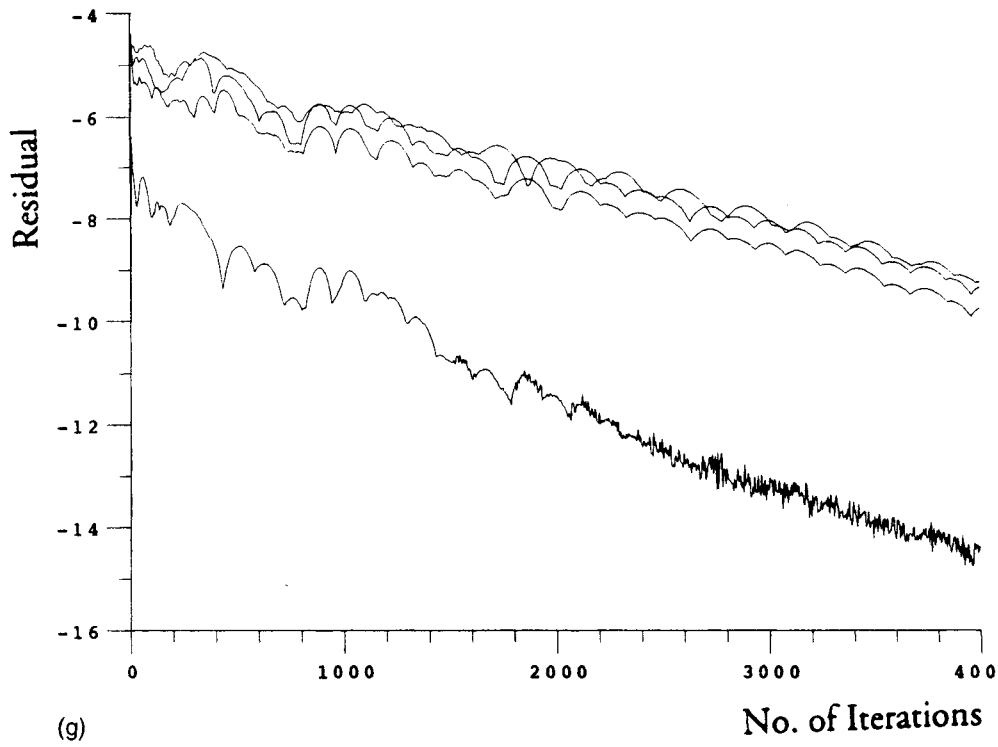

(g)

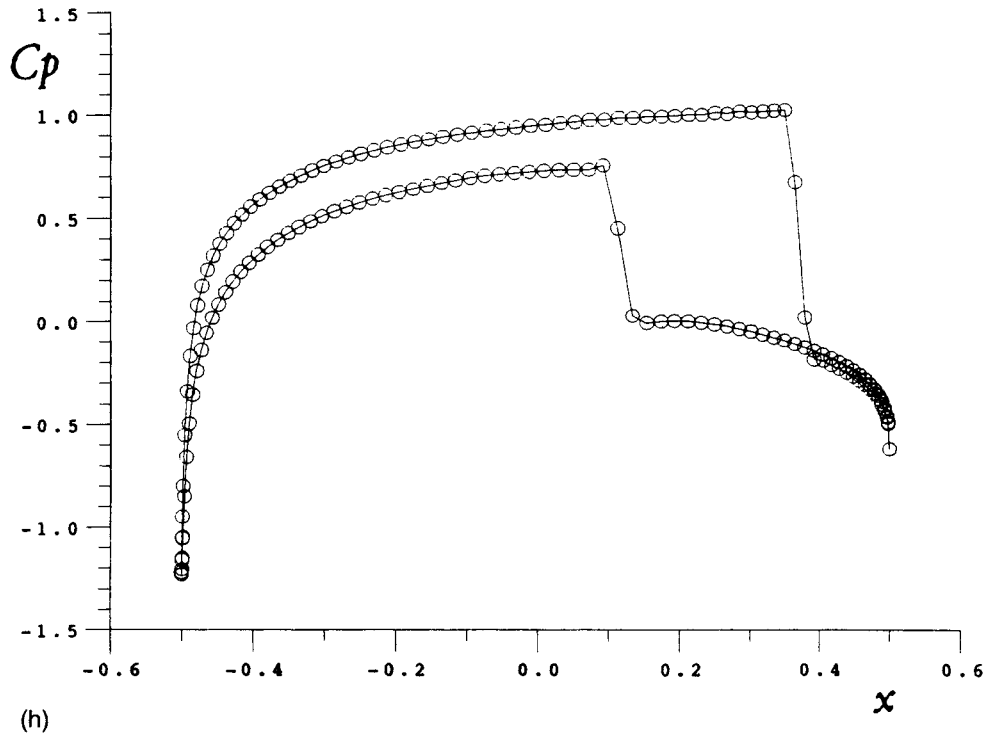

(h)

Figure 3. (g, h)

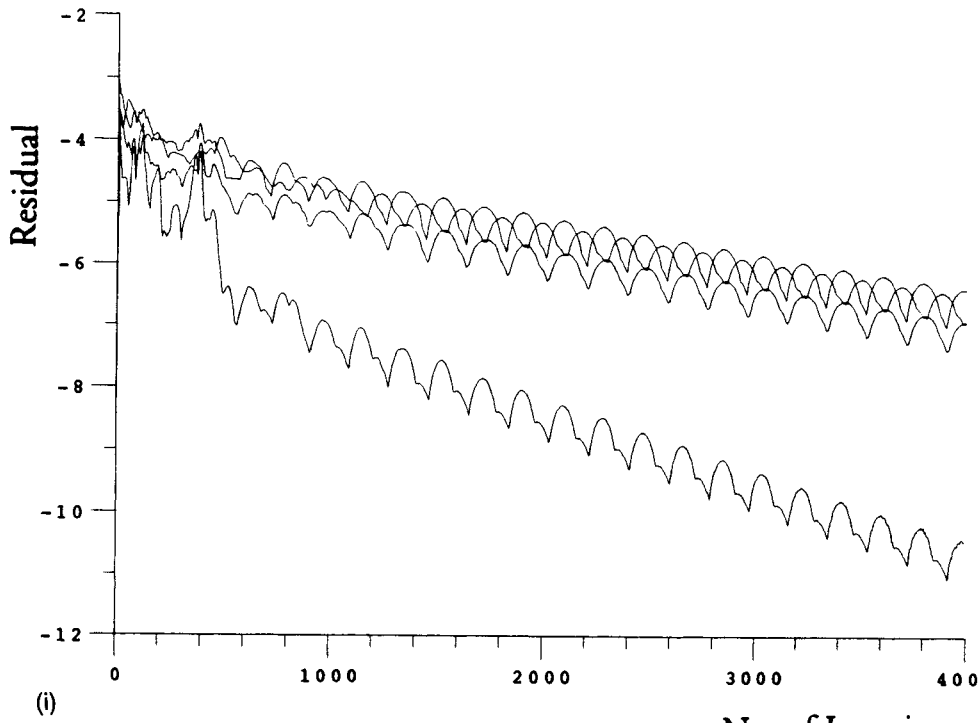

(i)

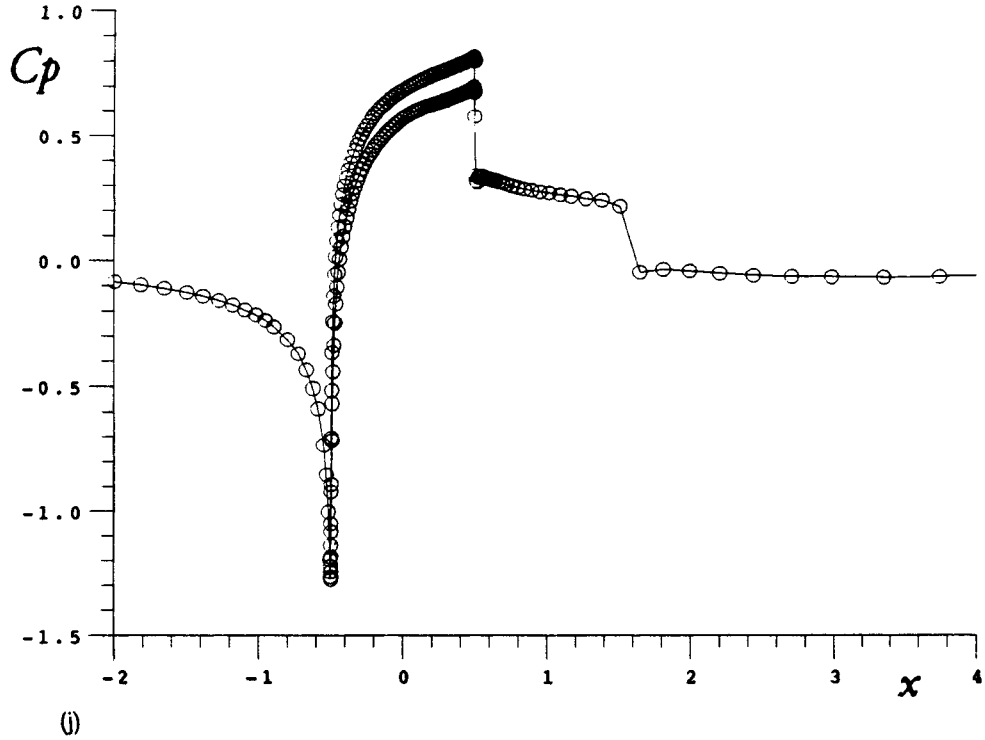

(j)

Figure 3. (i, j)

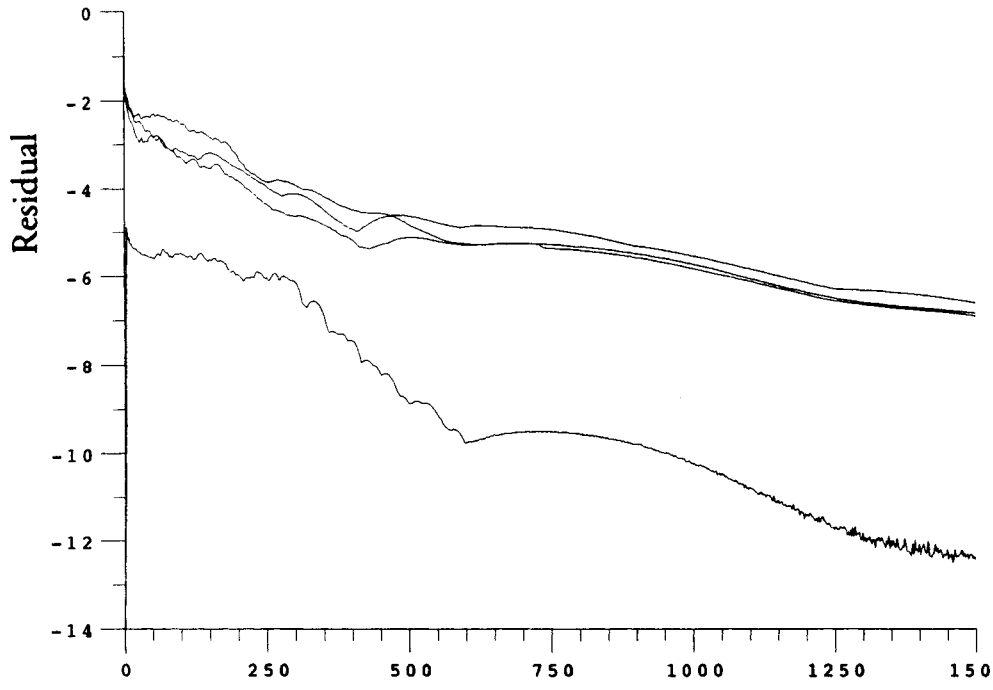

(k)

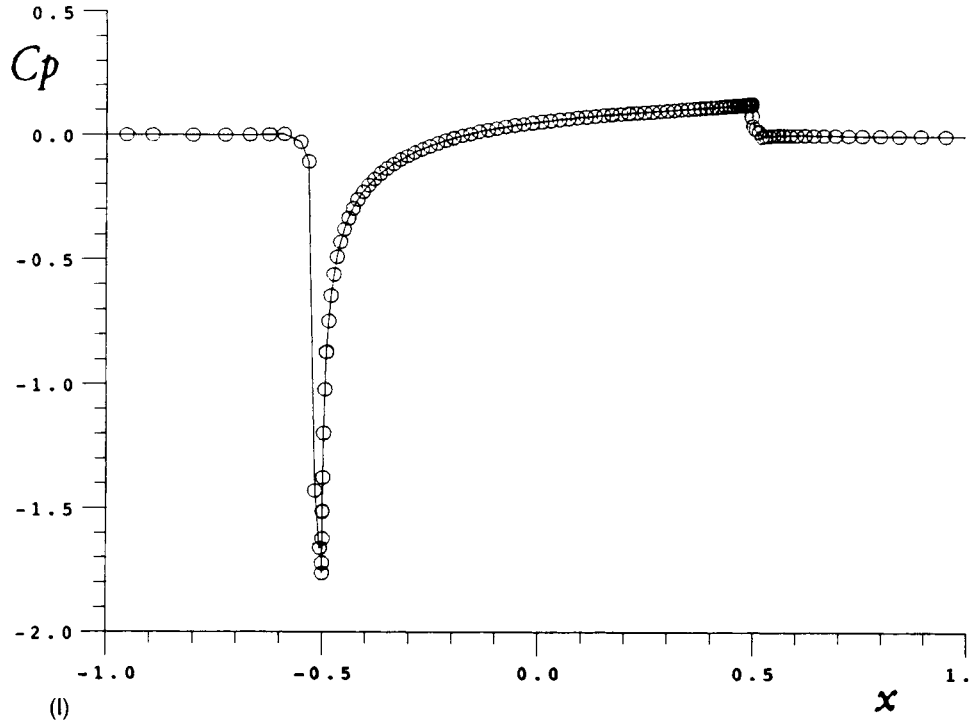

(l)

Figure 3. (k, l)

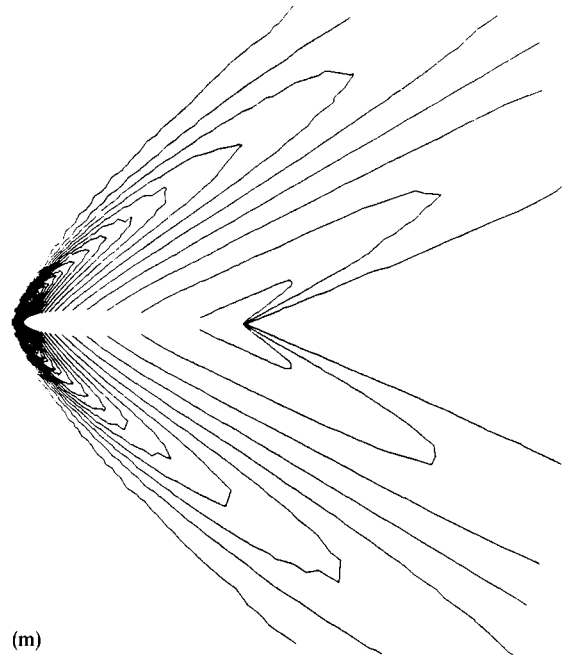

(m)

Figure 3. (a) Pressure contours, (b) surface pressure distribution, (c) history of the residuals, (d) surface pressure distribution for NACA 0012 aerofoil, Mach 0·2, 10°, (e) surface pressure distribution for NACA 0012 aerofoil, Mach 0·2, 20°, (f) surface pressure distribution for NACA 0012 aerofoil, Mach 0·8, 0°, (g) history of the residuals for NACA 0012 aerofoil, Mach 0·8, 0°, (h) surface pressure distribution for NACA 0012 aerofoil, Mach 0·85, 1·25°, (i) history of the residuals for NACA 0012 aerofoil, Mach 0·85, 1·25°, (j) surface pressure distribution for NACA 0012 aerofoil, Mach 0·95, 1·25°. (k) history of the residuals for NACA 0012 aerofoil, Mach 0·95, 1·25°, (l) surface pressure distribution for NACA 0012 aerofoil, Mach 2.0, 0° and (m) pressure contours for NACA 0012 aerofoil, Mach 2·0, 0°

of $M_\infty = 0{\cdot}85$ and $M_\infty = 0{\cdot}95$ with $\alpha = 1{\cdot}25°$ are plotted in Figures 3(h)–3(k). Finally, a supersonic case of $M_\infty = 2{\cdot}0$ at zero angle of attack is calculated and the pressure contours and surface distributions are shown in Figures 3(l) and 3(m). Notice the shock is smeared in the field; this is a common problem in most existing codes. Possible remedies include adaptive gridding and/or shock fitting.

4. SOLUTIONS OF NAVIER–STOKES EQUATIONS

This study is restricted to laminar flows where no turbulence modelling is required. Still, to resolve boundary layers, a stretched grid with a fine spacing in the neighbourhood of a solid surface is needed for practical calculations. (Uniformly fine mesh cannot be afforded). Unstructured grid generation, however, may lead to very distorted elements. Regular grids in the neighbourhood of the body may be preferred to allow for the thin layer approximation of Navier–Stokes equations, and for the implicit treatment of the unknowns in the direction normal to the wall. The flexibility of unstructured grid and the feasibility of its adaptation can be recovered outside the viscous layers. Hence, a hybrid grid maybe an optimal choice. An alternative will be oversetting grids, however, the interpolation may destroy the conservation of the numerical fluxes. Furthermore, an important issue in the calculations of high Reynolds number flows, is the use of artificial viscosity and the minimization of its effect relative to the real

viscosity. In this regard, schemes producing less artificial cross wind diffusion, are preferred. Unlike the artificial viscosity, accurate discretization of the real viscous terms is necessary. The accuracy deteriorates for stretched grids with very skewed elements calling in general for higher-order schemes. The present scheme is still however, applicable using linear elements.

Because of the no-slip boundary condition, the vorticity is concentrated in boundary layers and it is convected and diffused in the field. The pressure, unlike the velocity and vorticity does not have a large gradient in the direction normal to the wall and for high Reynolds numbers p_n is vanishingly small at the solid surface. For compressible flows, the energy equation should be solved (coupled with continuity and momentum equations) to obtain the temperature distributions and thermal boundary layers. Two non-dimensional parameters appear in the governing equations, Reynolds (*Re*) and Peclet (*Pe*) numbers. [The latter is the product of Prandtl (*Pe*) and Reynolds (*Re*) numbers.] The Mach number appears in the far-field boundary condition if the standard nondimensional formulation is adopted.

The governing equations for steady flows can be written in the following form:

$$\bar{\nabla}\cdot\bar{\rho}\mathbf{q} = 0 \tag{13}$$

$$\bar{\nabla}\bar{\rho}\mathbf{q}\mathbf{q} = -\bar{\nabla}\bar{p} + \frac{1}{Re}\bar{\nabla}\cdot\bar{\tau} \tag{14}$$

$$\bar{\nabla}\cdot\bar{\rho}\mathbf{q}\bar{H} = \frac{1}{Pe}\bar{\nabla}\cdot\bar{k}\bar{\nabla}\bar{T} + \frac{1}{Re}\bar{\nabla}\cdot\bar{\tau}\cdot\mathbf{q} \tag{15}$$

where $\bar{\tau}$ is the viscous stress tensor and $\bar{k}$ is the coefficient of heat conductivity, normalized by its free stream value. The density and the velocity are normalized by their magnitude at free stream conditions. The pressure is normalized by $\rho_\infty q_\infty^2$, the temperature by q_∞^2/c_p and all distances by a characteristic length l. The perfect gas law, $p = \rho RT$, in non-dimensional form becomes

$$\bar{p} = \bar{\rho}\bar{T}\left(\frac{\gamma - 1}{\gamma}\right) \tag{16}$$

where

$$\bar{p}_\infty = \frac{P_\infty}{\rho_\infty q_\infty^2} = \frac{1}{\gamma M_\infty^2} \tag{17}$$

$$\bar{T}_\infty = \frac{T_\infty}{q_\infty^2/c_p} = \frac{1}{(\gamma - 1)M_\infty^2} \tag{18}$$

At a solid surface the velocity vanishes and either the temperature or its normal derivative is specified. In the far field, all disturbances vanish for subsonic flows, except in the wake. The ambient pressure is recovered far downstream of the body. For supersonic flows, disturbances propagate along preferred directions (characteristics) and the flow upstream of the body is undisturbed.

For convenience, some simplifications are made. The bulk or second viscosity coefficient is assumed to be zero. Both viscosity and heat conductivity coefficients are assumed constant and so are the specified heats c_p and c_v, and their ratio γ. It is well known that, compressible boundary layers equations admit a solution with constant total enthalpy (if $Pr = 1$). Outside the viscous layers, the total enthalpy is constant for inviscid adiabatic flows, with uniform upstream conditions. Hence, the energy equation can be replaced by the condition that the total enthalpy is constant everywhere. This is not an exact solution of the compressible Navier–Stokes equations but it is a reasonable approximation.

Numerical methods and results

As in Euler calculations, the continuity equation is augmented by the Laplacian of the pressure balanced by extra terms. The contributions of the viscous stresses in the momentum equations to these extra terms are neglected. Such an approximation is acceptable for high Reynolds number flows.

The momentum equations are also changed with augmented terms, similar to those used in Euler calculations. These terms, however, do not vanish on the differential level for viscous flows. Upon proper discretization, they produce higher-order streamwise artificial dissipation which is relatively small compared to the real dissipation. Furthermore, they are scaled with the speed, hence they are not contaminating the solution in the neighbourhood of a solid surface.

The above formulation is implier than the Taylor/Galerkin or full least squares. Application of the latter to Navier–Stokes equations leads to an equivalent system of biharmonic equations. Although, the appearance of fourth-order derivatives may be avoided by introducing extra unknowns, the corresponding calculations are still more expensive.

Here, Gauss theorems are used to integrate the augmented equations over the control volume and reduce the discretization process to approximation of line integrals. A proper treatment of boundary conditions is essential particularly at the solid surface. Both velocity components are set to zero at the boundary nodes. The pressure is obtained from the discretization of the normal momentum equation over the special control volumes near the boundary. (This treatment is more consistent than extrapolating the pressure or imposing $p_n = 0$ at the boundary nodes.) For more details see References 26 and 27. The density is obtained based on the condition of constant total enthalpy.

Viscous compressible flows over a lifting aerofoil (NACA 0012) at 10° is computed for $M_\infty = 0{\cdot}8$ and $Re = 500$ as well as for $M_\infty = 2{\cdot}0$ and $Re = 106$. Both calculations are performed on a 199×35 grid, and the results are plotted in Figure 4. In Figure 4(a) the surface pressure distribution of the first case is compared with Hollanders' solution.[28] The pressure contours are plotted in Figure 4(b). The pressure contours for the supersonic case is plotted in Figure 4(c). The results are in agreement with those of Reference 29. The same two cases are recalculated based on the zonal approach as will be discussed later.

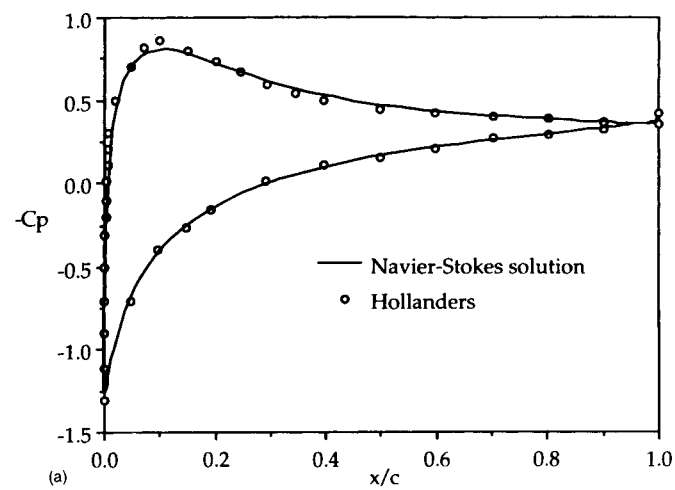

Figure 4. (a)

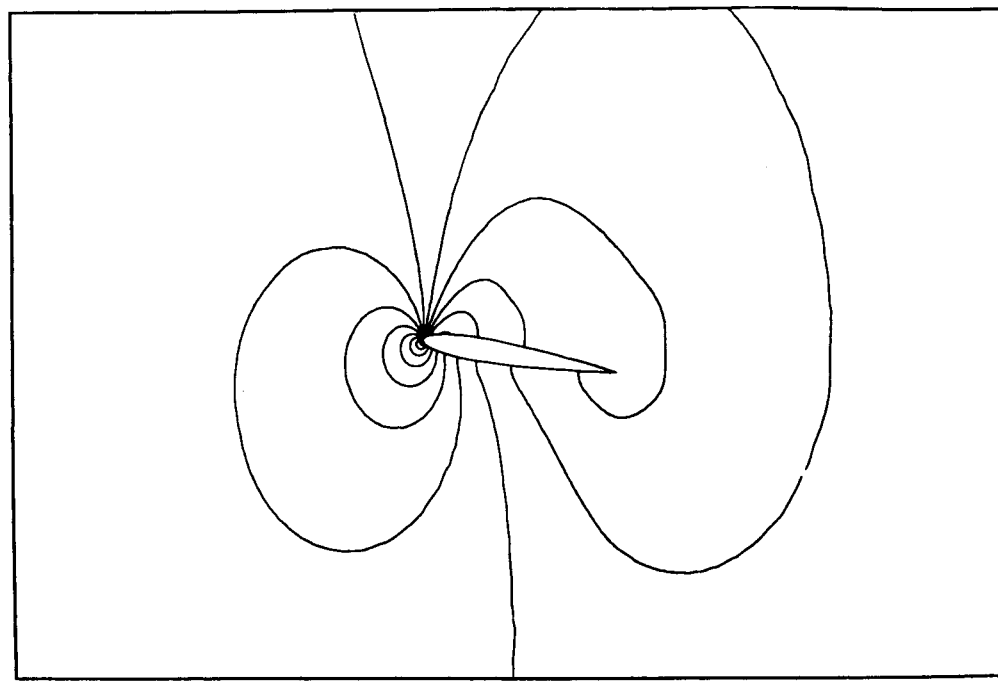

(b)

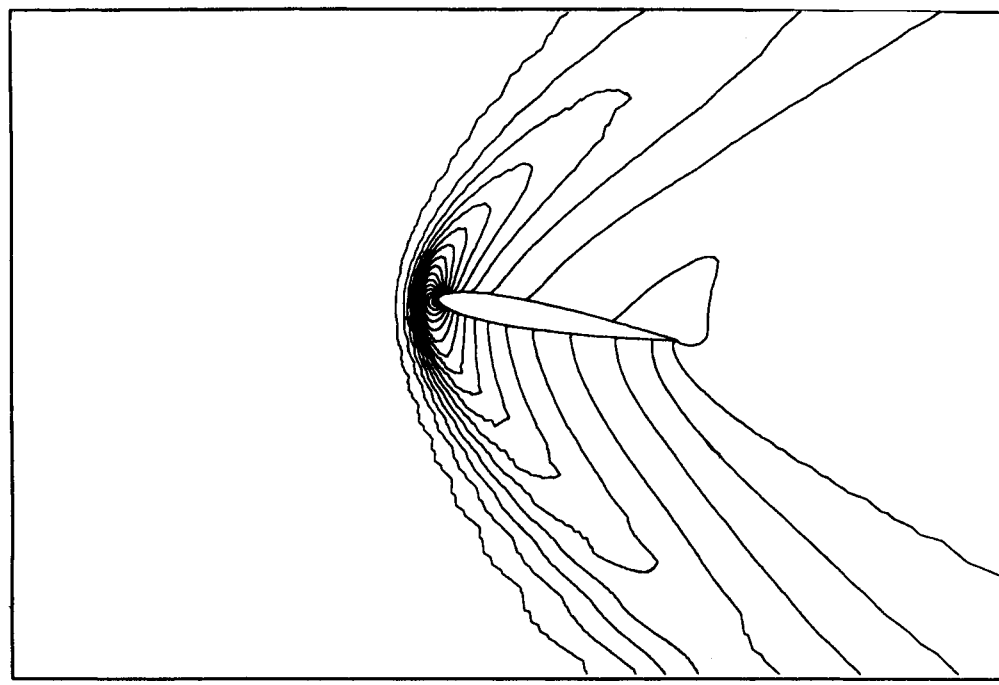

(c)

Figure 4. (a) Surface pressure distribution for NACA 0012 aerofoil, Mach 0·8, 10°, $Re = 500$, (b) pressure contours for NACA 0012 aerofoil, Mach 0·8, 10°, $Re = 500$ and (c) pressure contours for NACA 0012 aerofoil, Mach 2·0, 10°, $Re = 106$

The incompressible limit of the compressible Navier–Stokes equations. The performance of most of compressible codes in terms of a accuracy and convergence degenerates as the Mach number approaches zero and usually a separate incompressible code is needed for this special case. There are three obvious reasons behind this problem:

1. *Choice of variables*: usually conservative (ρ, ρu, ρv, pE) or primitive (ρ, u, v, p) variables are used in compressible codes. The density is not a variable in incompressible flows.
2. *Choice of references for non-dimensional variables*: for example, in some codes the velocity is normalized by the speed of sound at free stream conditions, which is unbounded for incompressible flows.
3. *The limit behaviour of the perfect gas law*: The pressure is not proportional to the temperature for constant density flows. On the contrary, the pressure is independent of temperature for this case.

In References 30 and 31 we proposed to use p, u, v, and T as variables. This choice is reasonable for the representation of both compressible and incompressible flows. The non-dimensional pressure and temperature become unbounded as the free stream Mach number vanishes, hence new bounded variables are introduced:

$$p^* = \bar{p} - \bar{p}_\infty = \bar{p} - \frac{1}{\gamma M_\infty^2} \tag{19}$$

and

$$T^* = \bar{T} - \bar{T}_\infty = \bar{T} - \frac{1}{\gamma - 1}\frac{1}{\gamma M_\infty^2} \tag{20}$$

With this choice, an expression for, the non-dimensional density can be easily obtained, since

$$\begin{aligned} \bar{\rho} &= \frac{\gamma}{\gamma - 1}\frac{\bar{p}}{\bar{T}} \\ &= \frac{\gamma}{\gamma - 1}\left(\frac{P^* + \dfrac{1}{\gamma M_\infty^2}}{T + \dfrac{1}{\gamma - 1}\dfrac{1}{M_\infty^2}}\right) \\ &= \frac{\gamma M_\infty^2 P^* + 1}{(\gamma - 1)M_\infty^2 T^* + 1} \end{aligned} \tag{21}$$

It is clear that $\bar{\rho}$ approaches 1 as the M_∞ approaches zero. Hence, the continuity, momentum and energy equations are solved for $\bar{\mathbf{q}}$, p^* and T^* and the density is replaced by its expression in terms of p^* and T^*. Notice, the same procedure is applicable for unsteady flows with uniform upstream conditions. The momentum and energy equations do not change if $\bar{p}$ and $\bar{T}$ are replaced by p^* and T^* since the differences are pure constants and only the derivatives of these variables with respect to space or time appear in the equations. Other formulations are studied for nonisothermal flows with a general gas law in Reference 31.

To demonstrate the validity of the new formulation, a general code was developed and tested for finite and zero Mach numbers. A simple test case of an incompressible viscous flow over a flat plate at high Reynolds number was calculated and the results were comparated with Blasius' boundary layer solution. The same code with supersonic free stream Mach number produced

a shock wave at the leading edge of the plate (due to the displacement thickness effect). In these calculations, the governing equations are augmented with extra terms, for example a Laplacian of p^* and the corresponding balancing terms are added to the continuity equation.

5. A ZONAL APPROACH FOR SIMULATION OF HIGH REYNOLDS NUMBER FLOWS

Recently, many attempts have been made to develop efficient strategies for simulation of high Reynolds number flows. Viscous/inviscid interaction procedures and zonal approaches are among the most promising methods. In viscous/inviscid interaction procedures, coupling the boundary layer and potential or Euler calculations provides a practical approximation for the solution of Navier–Stokes equations. The efficiency of the simulation depends, however, on the coupling strategy. Convergence difficulties are encountered for problems with large or massive separation. In the standard zonal approach, the viscous terms in Navier–Stokes equations are switched off outside a thin layer around the body and its wake. Hence, Euler equations are solved in most of the domain. The switching strategy must be chosen so it does not upset the convergence of the iterative solution process. Also, such an approach does not result in significant savings over a standard Navier–Stokes simulation.

In the present zonal approach, following the work of Tang and Hafez[26] (see also Reference 27), a simple coupling strategy between the inner (viscous) and outer (inviscid) zones is implored. The viscous effects are transferred to the inviscid calculations through a forcing function. More precisely, a thin layer is identified around the body and its wake where the viscous forces are important. The Navier–Stokes equations are solved only in these layers where the edge conditions are evaluated from a separate 'modified' inviscid calculation. The latter extends from the body surface to the far field covering the entire computational domain. The inviscid equation is augmented with a forcing function which is active only in the viscous layers. This forcing function is simply the vorticity evaluated from the Navier–Stokes solution at the previous iteration. The density is also modified in the viscous layers using the entropy distribution from Navier–Stokes calculations. The augmented inviscid calculations is based on modified Cauchy/Riemann equations, hence Euler equations are avoided. The inviscid solution supplies new boundary conditions for the next Navier–Stokes calculation. This iterative process of viscous/inviscid interaction is repeated until convergence.

The present method has the following advantages. Navier–Stokes equations are not solved everywhere, they are limited only to the thin viscous layers. No displacement thickness is evaluated and no boundary layer assumptions nor solutions are employed. The viscous effects are transferred through the vorticity and entropy distributions in the viscous layers. Obviously, finite element/finite volume simulations on unstructured grids can be used for both the Navier–Stokes and the augmented inviscid calculations. In general, two completely different oversetting grids can be used for the viscous and inviscid calculations. The numerical methods can be tailored to each region to maximize the overall simulation efficiency.

The disadvantage of the present method lies in the calculation of the augmented inviscid equations over the entire domain. (The overlap between the inviscid and viscous regions is the whole viscous region.) The situation can be be improved if nested grids are used and the forcing function is averaged over a rarefied grid, where the inviscid solution is obtained. It can be argued that this inviscid solution still provides a reasonably accurate boundary conditions for Navier–Stokes calculations.

Numerical methods and results

For two-dimensional flows, the following equations are solved in the entire domain of computation:

$$(\rho u)_x + (\rho v)_y = 0 \tag{22}$$

$$u_y - v_x = -\omega \tag{23}$$

where

$$\rho = \rho_i e^{-S/R} \tag{24}$$

and

$$\rho_i = \left(1 - \frac{\gamma - 1}{2} M_\infty^2 (u^2 + v^{2-1})\right)^{1/(\gamma-1)} \tag{25}$$

Both ω and s vanish outside the viscous layers. Their distributions inside these layers are obtained from the Navier–Stokes solution.

While this formulation works well for subsonic and slightly transonic flows, convergence difficulties are encountered for supersonic flow simulations. To overcome this problem, the governing equations are casted into a hyperbolic system in an artificial time. The Cauchy/Riemann equations are solved for the velocity magnitude (q) and direction (θ) (see Reference 11 for a similar pseudo-unsteady approach). The system of equations

$$q_t - (\rho q \cos\theta) - (\rho q \sin\theta)_y = 0 \tag{26}$$

$$\theta_t - (q \cos\theta)_y + (q \sin\theta)_x = \omega \tag{27}$$

can be symmetrized. The inviscid equations are now appropriate for supersonic calculations. A special treatment at the stagnation point ($q = 0$) is necessary. Although multiplies of 2π can be added or subtracted to the angle without affecting the sine and cosine functions, the angles should be defined consistently while evaluating the derivatives of θ.

The above equations are augmented with artificial dissipation. Gauss and Stokes theorem are used to integrate the augmented equations over the control volumes. Special control volumes are encountered near solid surfaces. As before, discrete equations for each node can be readily obtained. These equations are linearzied using Newton's method and at each iteration, a linear system is solved either explicitly or implicitly.

To test this approach a transonic flow at $M_\infty = 0{\cdot}8$ and $Re = 500$ over NACA 0012 aerofoil at 10° angle of attack is calculated on a (199×35) grid using the above viscous/inviscid iteration procedure. The contours of the pressure after 5 cycles using the forcing function approach are plotted in Figure 5(a) and in the same figure, the viscous region is identified. The comparison of the surface pressure distribution with Navier–Stokes solution is shown in Figure 5(b). Finally, a viscous supersonic case is calculated for, $M_\infty = 2{\cdot}0$ and $Re = 106$. The corresponding surface pressure distribution is shown in Figure 5(c).

In the présent study, in both Navier–Stokes and zonal calculations, uniform flows (except in the wake) are assumed for outer boundary conditions. Substantial improvements can be obtained using asymptotic far-field solutions. In fact, one can identify three layers, viscous, non-linear inviscid and linear inviscid layers. The use of asymptotic solutions can reduce the domain of integration to only two layers.

Other benefits of the zonal approach can be exploited. For example, the division of the computational domain provides a natural way to use parallel computers for a large problem. By solving the viscous and inviscid equations on different processors, the zonal approach can reduce storage and computer time requirements.

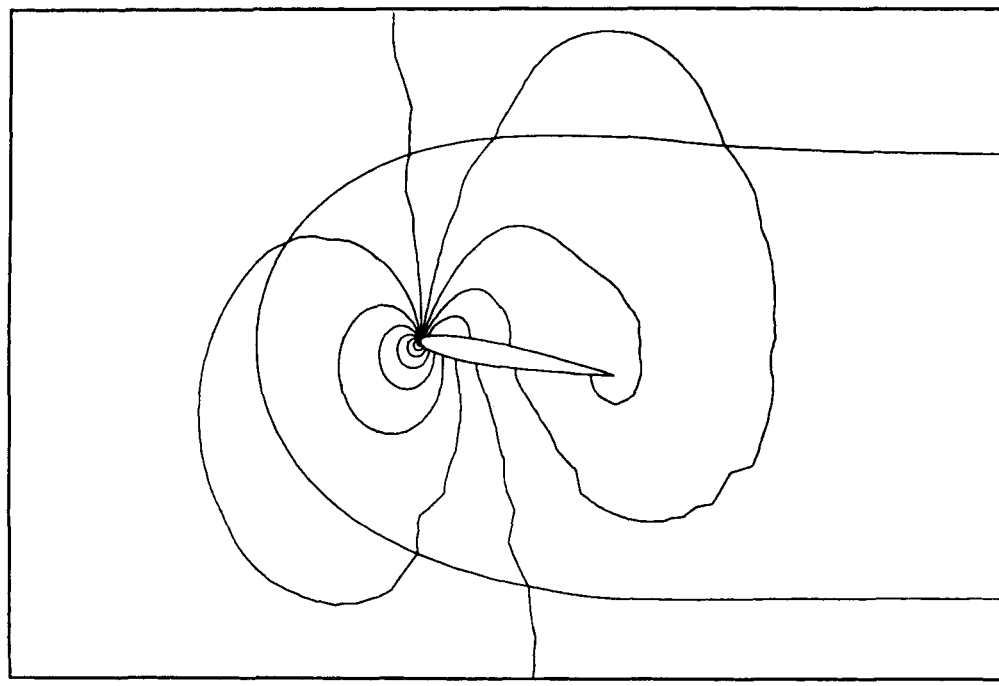

(a)

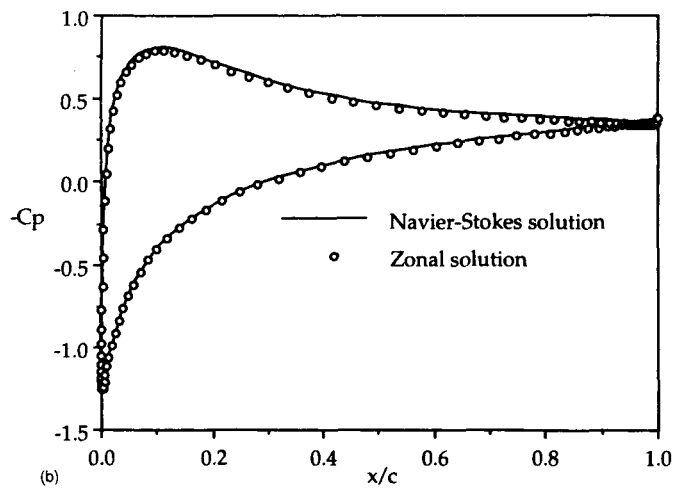

(b)

Figure 5. (a, b)

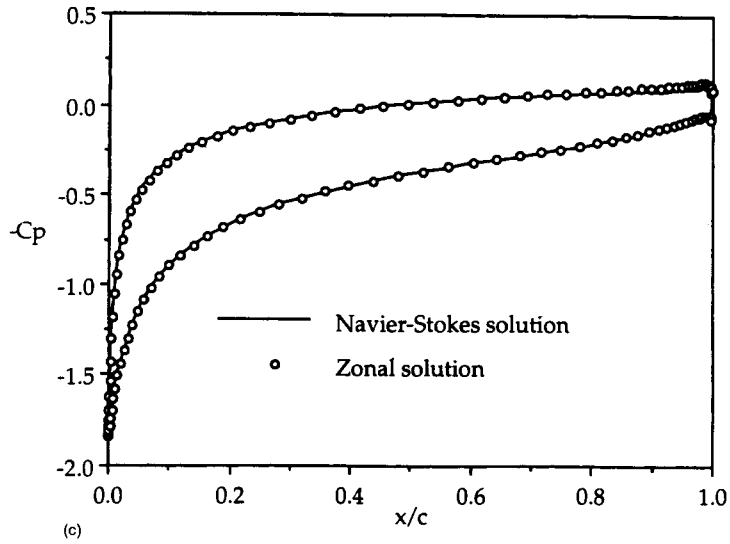

Figure 5. (a) Pressure contours for NACA 0012 aerofoil, Mach 0·8, 10°, $Re = 500$, (b) surface pressure distributions for NACA 0012 aerofoil, Mach 0·8, 10°, $Re = 500$, and (c) surface pressure distributions for NACA 0012 aerofoil, Mach 2·0, 10°, $Re = 106$

6. CONCLUDING REMARKS

In this paper some issues of the solutions of potential, Euler Navier–Stokes and Maxwell's equations are examined. For example, the non-uniqueness of the solutions of potential and Euler equations are discussed.(Although, up to the the author's knowledge, multiple solutions of Navier–Stokes equations, in the transonic regime, have not been demonstrated, non-unique solutions have been calculated by Bailey and Beam[37] for low subsonic-high Reynolds number flows).

Numerical results of a finite volume scheme based on a local finite element approximation are presented. (All calculations, in this work, are based on linear elements.) Higher-order artificial dissipation are produced upon the discretization of augmented higher-order terms consistent with the original equations. This development leads to compact schemes with natural boundary conditions hence only the physical constraints are imposed. The present scheme is simpler than those of least squares or Taylor/Galerkin methods, particularly in the case of viscous flow simulations. For the latter, preliminary results of a new zonal approach are promising. The incompressible limit of the compressible flow equations are studied and a unified formulation, valid for the zero Mach number case, is proposed.

More work is needed for the simulation of discontinuous solutions specially for the case of supersonic–supersonic shocks. Because of the artificial dissipation, the signature is lost few chords from the body. One remedy to this problem is grid adaptation, another possibility is shock-fitting.

Only calculations of steady-state solutions (except for Maxwell's equations) are considered. Extensions to time-dependent (transient) problems are not straightforward and are reported elsewhere.

ACKNOWLEDGMENTS

The numerical results presented in this paper for potential, Euler, Navier–Stokes, and Maxwell's equations were obtained by D. Kinney, R. Winterstein, C. Tang and P. English, respectively,

while they were graduate students at University of California, Davis. The author would like to thank T. Peraire, J. Perio and K. Morgan for the use of their 2D and 3D frontal grid generation packages.

APPENDIX

Solutions of Maxwell's equations

Recently, there has been an increasing interest in the numerical simulation of eletromagnetic wave propagation and scattering via time domain methods. Explicit time integration of Maxwell's equations has been successfully demonstrated by Taflove and Umshankar[32] using Yee's leapfrog method[33] and also by Shankar[34] using a Lax–Wendroff method. A staggered grid (in space and time) is employed with the leapfrog method, while there is, in general, a dissipation error with Lax–Wendroff method.

Since then, applications of CFD techniques to electromagnetic calculations has become popular. In this regard, one has to emphasize the differences between the two fields and promote this technology transfer only when it is relevant and promising. For example, in computational fluid dynamics, artificial viscosity methods, or upwind schemes, are commonly used to capture shock waves and contact discontinuities in the solution of the non-linear inviscid conservation laws (Euler equations). In contrast, Maxwell's equations are linear and amplitude and phase errors are of primary concern in wave propagation.

In the present study, a method is considered to overcome the decoupling of adjacent nodes on unstaggered grids without the deleterious effects of artificial viscosity. It is well known that Maxwell's first-order equations can be rewritten in the form of second-order wave equations for the electric and magnetic fields (assuming zero electrical conductivity and magnetic resistivity). The second-order form, however, requires more boundary (and initial) conditions. To supply these extra conditions, the first-order equations can be imposed on the boundary (provided that the boundary data is differentiable). For a smooth data and with proper treatments of the far field (radiation conditions) the two linear systems are equivalent and possess unique solutions which are identical (i.e. the solution of the first-order equations satisfy the second-order wave equations and vice versa). On the discrete level, using a staggered grid, it can be shown that the leapfrog method, applied to the first-order equations, is equivalent to the central difference scheme of the second-order wave equations, by taking the discrete curl of the first-order difference equations assuming the discrete electric and magnetic fields are divergence free. This argument is valid because the discrete version of a necessary vector identity holds on the staggered grid. Hence, for smooth data and smooth boundaries, one may replace the first-order Maxwell's equations by second-order wave equations and use the simple central difference scheme on unstaggered grids.

In general, it is still desirable to solve the original first-order equations. Applying central differences in space and time to the first-order equations leads to an explicit non-dissipative second-order accurate scheme. The solution, however, decouples over two sets of grid points and in Yee's method only one set of the grid points is considered and the other set is discarded.

In the present method, all the grid points are considered and to avoid the decoupling problems, the first-order equations are augmented with second-order derivatives, multiplied by a small parameter. Unlike the artificial viscosity methods, these augmented terms are not dissipative, and they vanish identically, on the differential level, for a smooth solution. The extra terms are simply the second-order wave equations. In short, a weighted combination of the first and second-order equations are solved on an unstaggered grid. Symbolically, the scheme can be written for the

vector unknown **W** in the form

$$L_1(\mathbf{W}) + \varepsilon L_2(\mathbf{W}) = 0 \tag{28}$$

where L_1 and L_2 are discrete approximations of the first- and second-order equations, respectively. Consider, for example, the simple wave equation

$$w_t + Cw_x = 0 \tag{29}$$

the corresponding augmented system is

$$w_t + Cw_x + \varepsilon(w_{tt} - c^2 w_{xx}) = 0 \tag{30}$$

The small parameter ε controls the properties of the discrete scheme. The scheme can be implemented on unstructured grids using finite elements or finite volumes in space and finite differences in time. Higher-order integration procedures in time for example Runge–Kutta method can be also used. Since Maxwell's equations can be written as a symmetric system of first-order hyperbolic equations, the present method can be related to either the least-squares/Galerkin or Taylor/Galerkin methods.

The two-dimensional transverse magnetic mode (TM) equations are solved for wave scattering off a cylinder and a NACA 0012 aerofoil following English and Hafez.[35] Equal order interpolation of the electric and magnetic fields are used. Applying Gauss and Stokes theorem reduces the integration of the augmented equations on a control volume to line integrals of the fluxes and their derivatives. At the bounded by nodes, the extra second-order terms are ignored and only the original equations are integrated over the special control volumes bounded by the object. For the TM mode, the electric field at the boundary of a perfectly conducting material and the normal component of the magnetic field vanish. The first condition is imposed explicitly while the second condition follows from the governing equations. The second boundary condition can be imposed implicitly as follows. As each boundary node, the normal and tangent to the body is calculated. The normal derivative of the electric field is calculated as a weighted combination of the

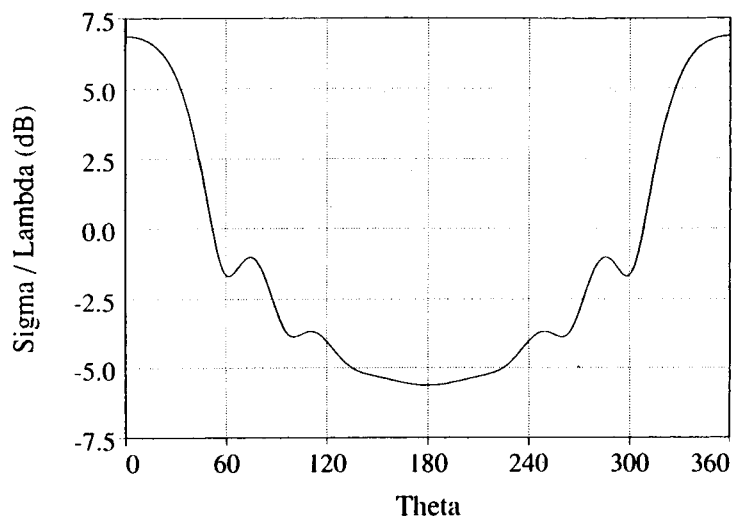

Figure 6. Bisatic RCS for circular cylinder

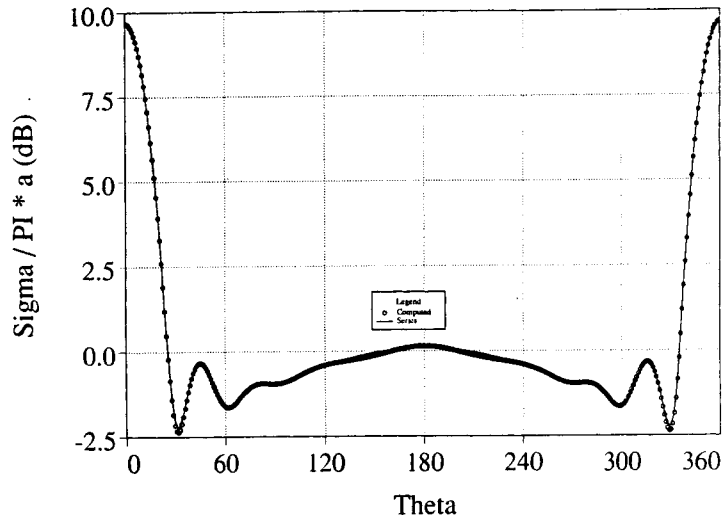

Figure 7. Bisatic RCS for NACA 0012 aerofoil

corresponding x and y derivatives in each element hence the tangential component of the magnetic field is updated and its x and y components are readily calculated. In the far field, a non-reflecting boundary condition is used. In the present calculations, both the first- and second-order time derivatives are discretized via central differences for all interior nodes. For the boundary and far field nodes, one sided differences are used. The scheme is explicit with a stability restriction on time step. For the cylinder a grid of 80 nodes on the body and 50 rings was used for an electrical size $ka = 5$. RCS were generated after 7·96 cycles ($\Delta t = 0{\cdot}01$). For the aerofoil, a grid of 116 nodes on the body and 70 rings was used for a wavelength of $2\pi l$, where l is the chord. The results were generated after 5·57 cycles ($\Delta t = 0{\cdot}001$). In Figure 6. Bistatic RCS for the circular cylinder is plotted and the numerical results are compared to a series solution. The corresponding results for the aerofoil is plotted in Figure 7. Higher-order schemes in space and time are discussed in Reference 36.

REFERENCES

1. V. Selmin, 'The node-centered finite volume approach: bridge between finite differences and finite elements', *Comput. Methods Appl. Mech. Eng.*, **102**, 107–138 (1993).
2. R. Pelz and A. Jameson, 'Transonic flow calculations using triangular finite elements', *AIAA Paper 83-1922.*
3. M. R. Bieterman, J. E. Bussoletti, C. L. Hilmers, W. P. Huffman, F. T. Johnson, R. G. Melvin and D. P. Young, 'Boundary layer coupling in a general configuration full potential code', *2nd European CFD Conf.*, Stuttgart, Germany, September 1994.
4. D. Kinney, J. Gloudemans and M. Hafez, 'The finite element solution of the full potential equation over aircraft configurations using unstructured tetrahedral and prismatic grids', *AIAA Paper 94-1928.*
5. D. Kinney, *Ph.D. Thesis*, UCD, 1994.
6. J. Peraire, J. Perio and K. Morgan, 'FELISA SYSTEM', *Reference and User's Manual*, December, 1993.
7. S. Osher, W. Whitlow and M. Hafez, 'Entropy condition satisfying approximations for the full potential equations of transonic flow', *NASA TM 85751*, January 1984.
8. M. Hafez, S. Osher and W. Whitlow, 'Improved finite difference schemes for transonic potential calculations', *AIAA Paper 84-0092.*
9. A. Jameson, 'Artificial diffusion, upwind biasing, limiters and their effect on accuracy and multigrid convergence in transonic and hypersonic flow', *AIAA Paper 93-3359.*
10. H. A. van der Vorst and P. Sonneveld, 'CGSTAB: A more smoothly converging variant of CGS', *Technical Report 90-50*, Delft Univ. Netherlands, May 1990.

11. H. Viviand, *Pseudo-unsteady Methods for Transonic Flow Computations*, Lecture Notes in Physics, Vol. 141, Springer, Berlin, 1981.
12. A. Jameson, 'Airfoils admitting non-unique solutions of the Euler equations' *AIAA Paper 91.1625.*
13. M. Salas, R. Melnik and A. Jameson, 'A comparative study of the non-uniqueness problem of the potential equation', *AIAA Paper 83-1888.*
14. T. Pulliam, 'A computational challenge: Euler solutions for ellipses', *AIAA Paper 89-0464.*
15. M. Hafez and D. Brucker, 'Effects of aritificial vorticity on the discrete solution of Euler equations', *AIAA Paper 91-1553.*
16. R. Winterstein and M. Hafez, 'Euler solutions for blunt bodies using triangular meshes: artificial viscosity and numerical boundary condition', *AIAA Paper 93-3333.*
17. R. Winterstein, *M.S. thesis*, UCD, 1993.
18. A. Jameson, W. Schmidt and E. Turkel, 'Numerical solutions of the Euler equations by finite volume methods using Runge–Kutta time stepping schemes', *AIAA Paper 81-1259.*
19. R. MacCormack and A. Paullay, 'The influence of the computational mesh on accuracy for initial value problems with discontinuous or non-unique solutions,' *Comput. Fluids*, **2,** 339–361 (1974).
20. A. Lerat and J. Sides, 'Efficient solutions of the steady Euler equations with centered Implicit method,' *Tech. Paper, ONERA, 1988-128.*
21. J. Donea, 'A Taylor–Galerkin method for convective transport problems', *Int. j. numer. methods eng.*, **20,** 101–120 (1984).
22. T. Hughes, 'Galerkin/least squares procedures in CFD, in T. Chung and G. Garr (eds.), *Finite Element Analysis in Fluids*, Univ. of Alabama Press, Birmingham, 1989.
23. B. Jiang, and L. Povinelli, 'Least squares finite element methods for fluid dynamics', *NASA TM 102352. COMP89-23*, 1989.
24. G. Fernandez and M. Hafez, 'Finite element simulation of compressible flows with shocks', *AIAA Paper 91-1551.*
25. G. Baruzzi, W. Habashi, J. Guevremont and M. Hafez, 'A second order finite element method for the solution of the transonic Euler and Navier–Stokes equations', this Volume.
26. C. Tang and M. Hafez, 'Finite element/finite volume simulations of viscous flows based on a zonal Navier–Stokes formulation' in *Int. Workshop on Solution Techniques for Large-Scale CFD Problems*, Montreal, Canada, September 1994.
27. C. Tang, *M.S. Thesis*, UCD, 1994.
28. H. Hollanders and W. Ravalason, 'Resolution des equations de Navier Stokes en fluide compressible par methode implicite', *La Recherche Aerospatiale*, **1,** 23–46 (1986).
29. D. Mavriplis and A. Jameson, 'Multigrid solution of the Navier–Stokes equations on triangulr meshes', *AIAA J*, **28,** 1415–1425 (1990).
30. M. Hafez and T. Ahmed, 'Vortex breakdown simulation, Part III—compressibility effects', *4th Symp. on Num. and Phys. Aspects of Aerodynamics Flows*, Long Beach, CA, 1989.
31. M. Hafeza, M. Soliman and S. White, 'A unified approach for numerical simulation of viscous compressible and incompressible flows over adiabatic and isothermal walls', *5th Symp. on Num. and Phys. Aspects of Aerodynamics Flows*, Long Beach, CA, 1992.
32. A. Taflove and K. Umshankar, '*Review of FD–TD Numerical Modelings of Electronmagnetic Wave Scattering and Radar Cross Sections of Complex Objects*, W. Ston (ed.), IEEE Press, New York, 1989, pp. 107–117.
33. K. Yee, 'Numerical solution of initial value problems involving Maxwell's equations in isotropic media', *IEEE Trans. Antennas Propag.*, **AP-14,** 302–307 (1966).
34. V. Shankar, 'A Gigaflop performance algorithm for solving Maxwell's equations of electromagnetics', *AIAA Paper 91-1578.*
35. P. English and M. Hafez, 'Time domain calculations of electromagnetic wave propagation and scattering using finite volumes and triangular meshes', *Int. Symp. IEEE Antennas and Propagation Society*, Ann Arbor, Michigan, July, 1993.
36. R. English, *M.S. Thesis*, UCD, 1994.
37. H. Bailey and R. Beam, 'Newton's method applied to finite difference approximations for the steady-state compressible Navier–Stokes equations', *J. Comp. Phys.*, **93,** 108–127 (1991).